Small-Amplitude Backbone Motions of the Spin-Labeled Lipopeptide Trichogin GA IV in a Lipid Membrane As Revealed by Electron Spin Echo

Victoria N. Syryamina,[†] Nikolay P. Isaev,[‡] Cristina Peggion,[§] Fernando Formaggio,[§] Claudio Toniolo,[§] Jan Raap,[||] and Sergei A. Dzuba*[,†,‡]

Department of Physics, Novosibirsk State University, 630090 Novosibirsk, Russia, Institute of Chemical Kinetics and Combustion, Russian Academy of Sciences, 630090 Novosibirsk, Russia, Department of Chemistry, University of Padova, 35131 Padova, Italy, and Leiden Institute of Chemistry, Gorlaeus Laboratories, University of Leiden, 2300 RA Leiden, The Netherlands

Received: July 21, 2010; Revised Manuscript Received: August 30, 2010

Trichogin GA IV is a lipopeptide antibiotic of fungal origin, which is known to be able to modify the membrane permeability. TOAC nitroxide spin-labeled analogues of this membrane active peptide were investigated in hydrated bilayers of 1-palmitoyl-2-oleoyl-sn-glycero-3-phosphocholine (POPC) by electron spin echo (ESE) spectroscopy. Because the TOAC nitroxide spin label is rigidly attached to the peptide backbone, it may report on the backbone orientational dynamics. The ESE signal in this system is observed below ~150 K. Previously, three-pulse stimulated ESE was found to be sensitive to two types of orientational motion of spin-labeled POPC lipid bilayers at these temperatures. The first type is fast stochastic librations, with a correlation time on the nanosecond scale (which also manifests itself in a two-pulse primary ESE experiment). The second type is slow millisecond inertial rotations. In the present work, we find that at low molar peptide to lipid ratio (1:200), where the individual peptide molecules are randomly distributed at the membrane surface, the spin labels show only a fast type of motion. At the high molar peptide to lipid ratio (1:20), a slow motion is also observed. Because at this high concentration trichogin GA IV is known to change its orientation from the in-plane topology to the transmembrane disposition, the observed onset of a slow motion may be safely attributed to the dynamics of peptides, which are elongated along the lipid molecules of the membrane. The possible interrelation between this backbone rotational motion of the peptide antibiotic and the membrane leakage is discussed.

Introduction

Trichogin GA IV, isolated from the mold *Trichoderma longibrachiatum*,[1] belongs to the class of lipopeptaibol[1−3] antibiotics. This amphipathic peptide is characterized by a sequence of 10 amino acids, a high proportion of the helicogenic α-aminoisobutyric acid (Aib) residues,[4−6] a 1,2-amino alcohol at the C-terminus, and a lipophilic *n*-octanoyl group at the N-terminus.[1−3] Trichogin GA IV exhibits remarkable membrane-modifying properties (for review articles, see refs 2, 3, and 7), leading to bacterial cell death probably due to collapse of the transmembrane electrochemical gradient.[8] In a recent study of a fluorescent derivative of trichogin GA IV, a strong correlation was found between the liposome content leakage and the concentration of membrane-bound peptide aggregates.[9] Compared with other peptaibols,[10] like the much longer 19-mer alamethicin,[11,12] which are believed to assemble to form transmembrane channels, trichogin GA IV is too short to span the membrane fully.

The orientation of trichogin GA IV in the membrane was studied using electron paramagnetic resonance (EPR)[13,14] or fluorescence[15,16] of properly labeled molecules and by solid-state NMR and FT-IR absorption.[17] From these studies it was concluded that at low peptide concentration the molecules acquire an in-plane orientation in the membrane. At high concentration, the orientation is changed to the transmembrane arrangement.[14,16] Also, at high concentration, aggregation of the peptide molecules does take place.[13,14,16] In this connection, pulsed electron−electron double resonance (PELDOR) data favor a pairwise type of aggregation.[14]

Despite the large number of studies, the molecular details of the mechanism by which this lipopeptaibol alters the permeability of membranes are still open for discussion. A physicochemical aspect that has not been paid much attention to is the dynamic behavior of this peptide when bound to the lipid membrane in the monomeric as well as in the aggregated states.

Modern spin-label EPR techniques using the spin active 4-amino-1-oxyl-2,2,6,6-tetramethylpiperidine-4-carboxylic acid (TOAC)[18] residue have emerged as powerful tools for determination of the peptide conformation, type of association to the lipid bilayer, and characteristics of the peptide aggregate, that is, the number of molecules per aggregate and the distances between the spin labels within the individual aggregated peptide molecules. The important advantage of this TOAC nitroxide label is that (compared with the much more flexible 1-oxyl-2,2,5,5-tetramethylpyrroline-3-methyl-methanethiosulfide/cysteine spin label, currently extensively used in protein studies) it reports directly the motion of the peptide backbone due to its rigid attachment.[19]

In the present Article, we apply three-pulse stimulated electron spin echo (ESE) technique to obtain information about the dynamics of the monomeric and aggregated trichogin GA IV in the membrane-bound state. Stimulated ESE is generated after

* Corresponding author. E-mail: dzuba@ns.kinetics.nsc.ru.
[†] Novosibirsk State University.
[‡] Russian Academy of Sciences.
[§] University of Padova.
[||] University of Leiden.

10.1021/jp106769q
Published on Web 09/08/2010

application of three microwave $\pi/2$ pulses to a spin system stored along the external magnetic field, in a time sequence denoted as $\pi/2 - \tau - \pi/2 - T - \pi/2 - \tau - echo$. As it has been recently shown,[20,21] the stimulated echo signal decay enables a direct observation of the orientational motion of two types. The first type is characterized by fast stochastic molecular librations (i.e., stochastic orientational oscillations of the whole molecule or of its segment; sometimes they are also called quasi-librations[22]), with correlation times on the nanosecond scale. The echo decay due to this mechanism exponentially depends on the time delay τ and does not depend on the time delay T. (Thus, two-pulse primary ESE, for which formally $T = 0$, is also sensitive to this type of motion.) The second type of motion is defined by slow millisecond inertial rotations, experimentally manifested in the accessible microsecond time scale by the reorientation of the nitroxide spin label within an angular range between ~0.1 and ~2°. These two limits are determined by the condition that the echo decay is too slow or too fast, respectively. For slow rotations, the echo exponentially depends on the product τT. Both types of motions manifest themselves in phospholipid bilayers at cryogenic temperatures, where spin relaxation is slow enough to observe the echo signal.[20,21] Although it is far below the physiological temperatures, such studies have the advantage that they may help to distinguish different motional mechanisms.

In this work, two synthetic analogues of trichogin GA IV have been investigated, which primary structures are listed below. In these analogues, one of the three aminoisobutyric acid (Aib) residues is replaced by the TOAC spin label, whereas the native C-terminal 1,2-aminoalcohol leucinol (Lol) is replaced by its synthetic precursor leucine methyl ester (Leu-OMe), and the N-terminal *n*-octanoyl (*n*Oct) group is replaced by the equally hydrophobic, but fluorescent, fluorenyl-9-methyloxy-carbonyl (Fmoc) group.

*n*Oct-Aib[1]-Gly-Leu-Aib-Gly-Gly-Leu-Aib[8]-Gly-Ile-Lol (trichogin GA IV)

Fmoc-**TOAC**[1]-Gly-Leu-Aib[4]-Gly-Gly-Leu-Aib[8]-Gly-Ile-Leu-OMe (FTOAC1)

Fmoc-Aib[1]-Gly-Leu-Aib[4]-Gly-Gly-Leu-**TOAC**[8]-Gly-Ile-Leu-OMe (FTOAC8)

It is known that these replacements do not alter the 3D-structural properties or the membrane activity of trichogin GA IV.[1-3] All peptides were studied in hydrated 1-palmitoyl-2-oleoyl-sn-glycero-3-phosphocholine (POPC) membranes at different peptide-to-lipid molar ratios.

The results obtained by stimulated ESE spectroscopy show that the increase in peptide concentration results in the onset of slow rotations. This observation may provide new insight into the mechanism of the membrane-modifying properties of trichogin GA IV.

Materials and Methods

Sample Preparation. The syntheses and characterizations of the spin-labeled trichogin GA IV analogues FTOAC1 and FTOAC8 were already described.[13,23] Hereafter we denote the unlabeled peptide trichogin GA IV as *P*, spin-labeled analogues as P_{SL}, and POPC lipids as *L*. For each spin labeled analogue, three types of samples were prepared, with $P_{SL}/P/L$ molar ratios of 1:0:200, 1:9:200, and 10:0:200. The first ratio represents peptide-diluted samples, whereas the second and third ratios correspond to peptide-enriched samples. The first and second ratios are also spin-diluted, whereas the third one is spin-enriched. Peptides and lipids were codissolved in chloroform. The solvent was then removed by evaporation in vacuo, followed by hydration of the residue in water at room temperature. In some experiments, deuterium water was used for hydration. Then, the hydrated lipid bilayers were concentrated by pelleting in a benchtop centrifuge. The excess water was then removed until the final water concentration was decreased to ~50% w/w. Before measuring, the samples were incubated for 24 h at room temperature and then cooled by shock freezing at the liquid nitrogen temperature.

To prove that contact with deuterium water does not result in substitution of hydrogen by deuterium, control samples were prepared. FTOAC1 and FTOAC8 were separately dissolved in an equimolar mixture of D_2O and CD_3OH. The samples were stored at room temperature for 24 h. Then, solvent was removed by blowing nitrogen following by storage in vacuum for 4 h. After dissolving in an equimolar mixture of toluene and chloroform, the samples were placed in EPR tubes and frozen in the glass state at liquid nitrogen.

EPR Measurements. We used a Bruker ESP-580 FT EPR spectrometer equipped with a dielectric cavity (Bruker ER 4118 X-MD-5) inside an Oxford Instruments CF 935 cryostat. The cavity was critically coupled for acquisition of continuous wave (CW) EPR spectra and overcoupled for pulsed EPR measurements. The amplitudes of microwave pulses of 16 ns durations were adjusted to provide a $\pi/2$ turning angle (so making this amplitude approximately 6 G). The spectrometer dead time induced by cavity ringing after application of the pulse was typically 100 ns.

The cryostat was cooled by a cold flow of nitrogen gas. The temperature of the sample was monitored with a calibrated Cu-Constantan thermocouple placed directly in the sample tube. The temperature was maintained with an accuracy of ±0.3 K.

The ESE envelope modulation (ESEEM) experiments, followed by data analyses, were carried out as previously described.[14,24] The delay between the first and second pulses of the three-pulse stimulated echo pulse sequence was equal to 200 ns in all measurements. The ESEEM was recorded by scanning the T delay, starting from 248 ns with a step of 12 ns, up to 12 μs. The unwanted echoes were eliminated with a four-step phase cycling program. The temperature of measurements was kept at 78 K. Fourier transformation of time-domain data was performed numerically with a homemade computer program.[24] Note that the suggested data treatment[24] results in spectral densities that have absolute values and may be used for comparison of different D_2O-containing systems.

Data Analysis. For a nitroxide spin label experiencing fast stochastic librations around the X molecular axis with small reorientation angles, $\alpha(t) \ll 1$, the echo signal decays as[20]

$$E_{fast}(2\tau, T) \propto \exp(-2 < \alpha(t)^2 > R_X^2(\theta, \varphi)\tau\tau_c) \qquad (1)$$

where

$$R_X(\theta, \varphi) = \gamma\left[B(g_{YY} - g_{ZZ}) + \frac{m(A_{YY}^2 - A_{ZZ}^2)}{(A_{XX}^2 \sin^2\theta\cos^2\varphi + A_{YY}^2 \sin^2\theta \sin^2\varphi + A_{ZZ}^2 \cos^2\theta)^{1/2}}\right] \times \cos\theta \sin\theta \sin\varphi$$

and where γ is the gyromagnetic ratio, τ_c is the motional correlation time, θ and φ are the angles determining the orientation of the magnetic field in the molecular framework, B is the magnetic field strength, g_{YY}, g_{ZZ}, A_{YY}, and A_{ZZ} are the principal values of the g tensor and the tensor of hyperfine interaction, and m is the projection of the nitrogen nuclear spin onto its quantization axis ($m = 0, \pm 1$). Fast motion means that $R_X^2(\theta,\varphi)\tau_c^2 < 1$. As for nitroxides at the X-band microwave frequency, the maximum $R_X(\theta,\varphi)$ value attains a magnitude of $\sim 3 \times 10^8$ s^{-1} (see also below); this condition means that τ_c lies on the nanosecond time scale. For a small-amplitude motion, the angles θ and φ in eq 1 may be considered as constants. When studying relaxation within a particular hyperfine structure component, m also may be taken as a constant. (See also below.) For motions around the two other molecular axes, Y and Z, a circular permutation in eq 1 has to be made of the subscripts X, Y, and Z, simultaneously with the polar coordinates sin θ cos φ, sin θ sin φ, and cos θ.

Note that eq 1 does not depend on the time delay, T. This is a property of fast motion, for which the magnetization evolutions during the two τ-intervals are statistically independent.

For the model of slow inertial rotations, in which the molecule freely rotates around the X molecular axis, with an angular velocity Ω during the experimental time interval, the echo decays as[20]

$$E_{\text{slow}}(2\tau, T) \approx \exp(-|R_X(\theta, \varphi)|\Omega_X(\tau^2 + \tau T)) \qquad (2)$$

where Ω_X is a parameter characterizing the width of the distribution function $g_X(\Omega)$ for motion around the X axis. (For different molecules, the Ω values may be different.) In the case of a Lorentzian distribution, Ω_X corresponds to the half width at the half-height of this distribution.

Both mechanisms given by eqs 1 and 2 result in an exponential decay when τ is varied. The rates of the decay are given by the formulas

$$W_{\text{fast}}^X = 2 < \alpha(t)^2 > R_X^2(\theta, \varphi)\tau_c \qquad (3a)$$

and

$$W_{\text{slow}}^X(T) = |R_X(\theta, \varphi)|\Omega_X T \qquad (3b)$$

respectively. In the latter case, it is taken into account that in a three-pulse stimulated echo experiment normally $T \gg \tau$. (See eq 2.)

If one assumes that these small-amplitude motions are isotropic (so that motion occurs independently around all three molecular axes),[20] then the total relaxation rate, instead of eq 3a, is

$$W_{\text{fast}} = W_{\text{fast}}^X + W_{\text{fast}}^Y + W_{\text{fast}}^Z \qquad (4a)$$

and

$$W_{\text{slow}}(T) = W_{\text{slow}}^X(T) + W_{\text{slow}}^Y(T) + W_{\text{slow}}^Z(T) \qquad (4b)$$

with the motional parameters $<\alpha(t)^2> \tau_c$ and $\Omega_{X(Y,Z)}$ being equal for motions around all three molecular axes.

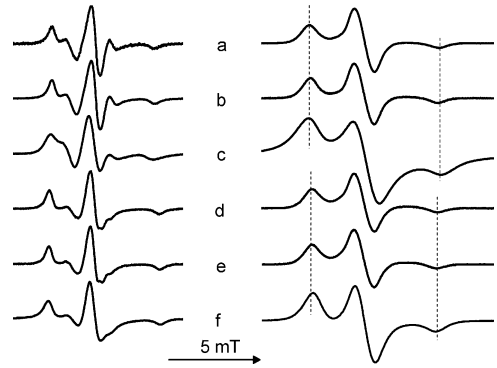

Figure 1. CW EPR spectra of spin-labeled trichogin analogues in a POPC bilayer taken at room temperature (left) and at 77 K (right): (a) FTOAC1, $P_{SL}/P/L$ is 1:0:200, (b) FTOAC1, 1:9:200, (c) FTOAC1, 10:0:200, (d) FTOAC8, 1:0:200, (e) FTOAC8, 1:9:200, and (f) FTOAC8, 10:0:200. The two pairs of dashed lines correspond to the positions of the outer spectral extremes for spectra at 77 K: for (a) − top pair, and for (d) − bottom pair.

Results

Figure 1 presents the CW EPR spectra of the six samples investigated in this work. The EPR lineshapes consist of three hyperfine structure components corresponding to three nitrogen spin projections on its quantatization axis ($m = 0, \pm 1$) and are determined by the anisotropy of the hyperfine interaction and of the g factor.

One may notice that for the FTOAC1, the total splitting between the two outer extremes decreases for a high peptide concentration (cf. Figure 1a,b, the observed decrease is ~0.15 mT), whereas for FTOAC8, it does not change within the experimental accuracy (cf. Figure 1d,e). Also, for the spin-enriched FTOAC1 sample (Figure 1c), the EPR hyperfine structure lines are remarkably broader as compared with the line widths of the five other spectra. All of these features are observed for both room and cryogenic temperatures.

To obtain information on the peptide orientation in the bilayer, we performed an ESEEM experiment employed previously for model membranes.[14,25,26] The basic concept of this experimental approach is that the Fourier transform of the ESEEM amplitude for bilayers hydrated by deuterium water reflects the distance from the headgroup region of the membrane where water is located. In measurements, the magnetic field was set to the maximum of the echo-detected EPR spectrum. Figure 2 shows the ESEEM spectra recorded for our samples. The peak observed at 2.2 MHz is induced by interaction of the unpaired electron of the spin label with deuterons. The doublet splitting of the peak is induced by quadrupole interaction of the deuterium nuclei. At the vertical axes in Figure 2, we use here the same absolute scale as that in ref 24. From Figure 2, it is clear that an increase in the peptide concentration (from $P_{SL}/P/L$ 1:0:200 to $P_{SL}/P/L$ 1:9:200) results in a noticeable drop of the line intensity in the case of FTOAC1, whereas in the case of FTOAC8, the intensity does not change. The analogous effect was previously observed for trichogin GA IV in a DPPC membrane.[14] It may be readily interpreted as a consequence of a change of the in-plane to the transmembrane peptide helix orientation, with a deeper insertion of the N-terminus (including the hydrophobic Fmoc group) into the membrane interior.

The echo signal was found only below 150 K; above this temperature, the echo decays were too fast. The echo signal decay was obtained with varying τ and keeping T fixed. The echo signal decay was obtained for two positions in the EPR spectrum. These two positions are indicated by arrows in the

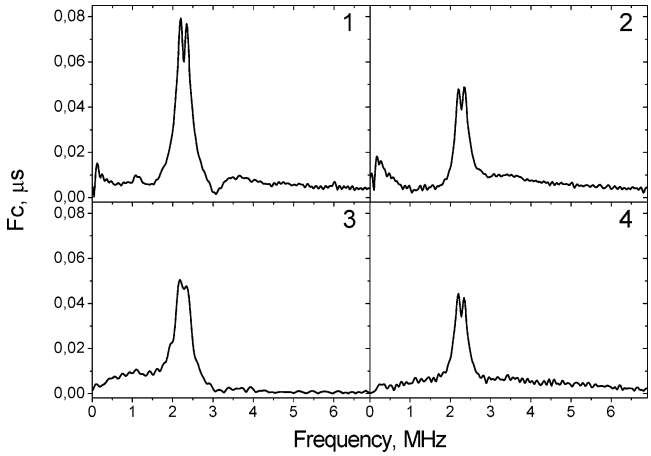

Figure 2. Modulus Fourier transform ESEEM spectra for D_2O-hydrated POPC bilayers. FTOAC1 − (1), (3); FTOAC8 − (2), (4). The molar ratios are: $P_{SL}/P/L$ 1:0:200 (1), (2); $P_{SL}/P/L$ 1:9:200 (3), (4).

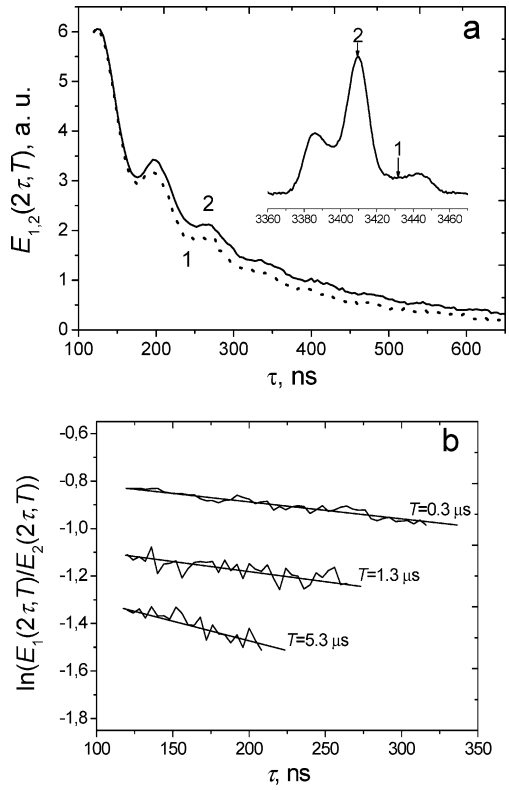

Figure 3. (a) Echo decay traces versus τ for $T = 1.3$ μs for two field positions 1 and 2 shown in the inset. The intensities at the beginning are artificially adjusted to the same value. (b) Semilogarithmic plot of the ratio of the traces taken at positions 1 and 2 at different time delays, T. For convenience, the data have been shifted arbitrarily along the vertical axis. Straight lines show linear fits of the data. The temperature is 109 K, and the sample is FTOAC8 in a POPC bilayer ($P_{SL}/P/L$ 1:0:200).

inset of Figure 3a, where a two-pulse echo signal ($\tau = 120$ ns, $T = 0$) is shown as a function of the magnetic field (a so-called echo-detected EPR line shape). These positions correspond to two limiting cases of anisotropy: the highest one for the first position and the lowest one for the second position. The comparison of the decays for these two positions allows refinement of the pure contribution of the orientational motion of the nitroxide from other sources of relaxation (mostly spin flips of nearby nuclei). Note, that this experiment is possible

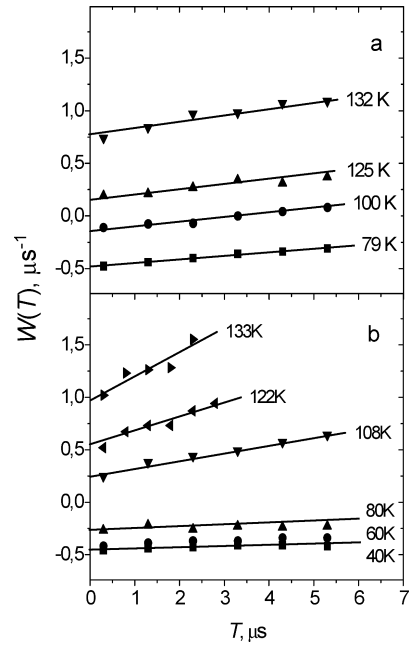

Figure 4. Relaxation rates $W(T)$ at different temperatures obtained as slopes of the straight lines like those shown in Figure 3b for FTOAC1 in a POPC bilayer. (a) Molar ratios $P_{SL}/P/L$ 1:0:200; and (b) $P_{SL}/P/L$ 1:9:200. The straight lines are linear fits of the data according to multiplication of eqs 3a and 3b (or eqs 4a and 4b).

only when the excitation bandwidth is much narrower than the total EPR line width. (In our case, these two values are 6 and 70 G, respectively.)

The echo decays as a function of τ given in Figure 3a show that a larger anisotropy results in a faster decay. Also, noticeable oscillations are seen in the decay curves (so-called ESEEM). To refine the contribution to the decay due to the orientational motion of the spin label, we numerically divided the time traces for the decays at the first field position by those at the second one. The results are given on a semilogarithmic scale in Figure 3b for three different T delays. Note that after this division ESEEM is essentially damped, which means that it is field-independent. Furthermore, one can see in Figure 3b that the echo decays are satisfactorily fitted by straight lines, which implies that the decays are exponential. Therefore, one may introduce the slopes of the lines as experimentally obtained decay rate parameters. These parameters have a clear meaning in the simple theory of molecular motion presented above; see eqs 3a and 3b. Because the slopes may depend on T, we denote them hereafter as $W(T)$.

Note also that this approach allows suppressing the influence on the resulting echo decay of the spin−lattice relaxation of the electron spins and of the spin flips of the nitrogen nuclei. As it was assessed in an inversion−recovery ESE experiment on spin-labeled lipids[27] (Figure 4 in ref 27), both of these processes, taken as relative decay rates for positions 1 and 2 in the spectrum, result in an effect that is negligibly small as compared with that induced by anisotropic relaxation in stimulated ESE.

Figures 4 and 5 show $W(T)$ as a function of T for the FTOAC1 and FTOAC8 samples, for the P_{SL}/P/L ratios equal to 1:0:200 and 1:9:200. One can see that all data in Figures 4 and 5 can be satisfactorily approximated by straight lines, with the intercepts at $T = 0$ increasing with temperature. For samples of a low peptide concentration (Figures 4a and 5a), the lines at all temperatures are parallel to each other. Also, they are nearly parallel to the horizontal axis, so the $W(T)$ values are practically

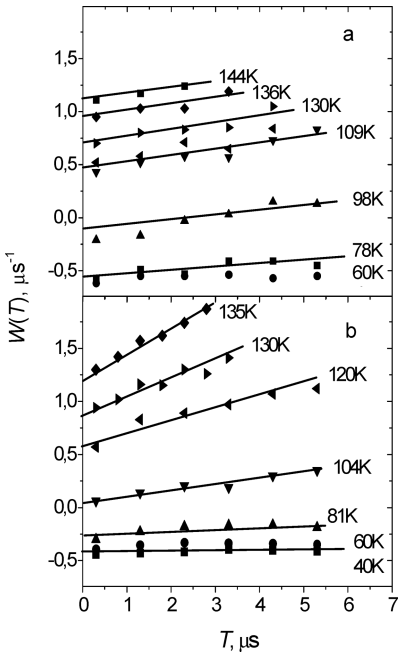

Figure 5. Same as in Figure 4 for FTOAC8.

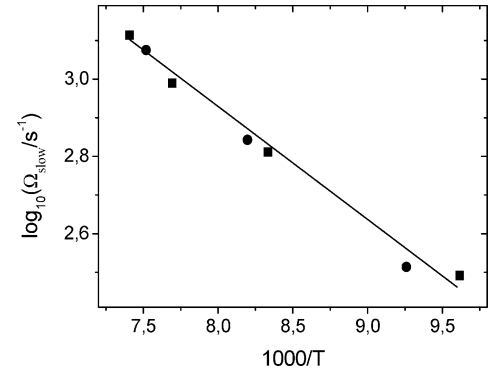

Figure 6. Arrhenius plot of the characteristic rotational frequencies, Ω_{slow}, obtained from data in Figure 4b for FTOAC1 (●) and in Figure 5b for FTOAC8 (■).

T-independent. In contrast, the $W(T)$ values determined at high peptide concentration (Figures 4b and 5b) certainly depend on T in a linear way, and the slopes of the linear dependences noticeably increase with temperature.

The negative $W(T)$ intercepts at $T = 0$ shown in Figures 4 and 5 may be readily explained by a so-called instantaneous diffusion process in ESE. This process is induced by alternation of the sign of the dipole−dipole interactions between different spin labels under the action of the microwave pulses. For nitroxide spin labels, the influence of the instantaneous diffusion process was quantitatively described in ref 28. Because of this process, the rate of the additional echo decay depends on the label concentration and is proportional to the fraction of excited spins. It is the highest for excitation of the component of lowest anisotropy, which does explain the appearance of the negative $W(T)$ values. It is important to note that the rate of the decay, due to the mechanism of instantaneous diffusion, is temperature-independent, thus presenting the sole contribution to $W(T)$ at low temperatures where motion is absent. One may conclude from the data in Figures 4 and 5 that there is no difference between $W(T)$ values obtained at 40 and 60 K. Therefore, 60 K may be considered to be the temperature where the motion becomes completely frozen out.

Previously,[20] it was shown that under the used experimental setup the $|R_X(\theta,\varphi)|$ and $|R_Y(\theta,\varphi)|$ values in eqs 1 and 2 may be safely replaced by a constant equal to 2.8×10^8 s^{-1}. As for nitroxides $|R_{X(Y)}(\theta,\varphi)| \gg |R_Z(\theta,\varphi)|$, the latter value in rough estimations may be neglected. Then, from the data in Figures 4 and 5, and by using eq 3a, the motional parameters $\langle\alpha(t)^2\rangle\,\tau_c$ and $\Omega_{X(Y)}$ may be obtained. (For a correct experimental determination of $W(T)$ values, one must exclude the influence of instantaneous diffusion. For that purpose, the found $W(T)$ value is to be subtracted from the corresponding value obtained at 40 or 60 K.) If we assume that our small-amplitude motion is isotropic, then eqs 4a and 4b must be used. Taking into account that motion around the Z axis only negligibly manifests itself, the experimental data on $W(T)$ are to be multiplied by a factor of 1.5. The results for slow motion are given in Figure 6 as an Arrhenius plot for two samples each at a molar ratio of 1:9:200. One can see that rotation of the molecule observed in the described experiment occurs on the millisecond time scale.

Note that at a high spin label concentration ($P_{SL}/P/L$ ratio, 10:0:200) the straight lines like those shown in Figures 4 and 5 were found to have a nonzero slope, even at low temperatures (data not given). This may be ascribed to a manifestation of spectral diffusion induced by a modulation of the dipolar interactions between the electron spins due to spin diffusion in the highly concentrated electron spin system. This process is expected to be temperature-independent as well, and these data showed an increase in the slope like those seen in Figures 4b and 5b for the peptide-concentrated, spin-diluted samples.

Discussion

The room-temperature CW EPR spectra of the membrane-reconstituted trichogin GA IV analogues (nitroxide-labeled at different positions), recorded at low peptide concentration, are similar to those normally shown for membrane-bound proteins.[29] As it was mentioned, the CW EPR line shape of the FTOAC1 sample at high spin and peptide concentration (Figure 1c) is noticeably broader, as compared with other samples. This line broadening is also observed at cryogenic temperatures, so it may occur only because of dipole−dipole interaction of the electron spins of the monolabeled peptides. This result is unambiguous evidence that spin labels at the N-terminals are nearby located in the aggregate at high peptide concentration. (See also below.)

In our previous ESE studies of spin-labeled stearic acid[20] and spin-labeled phospholipids[21] in POPC bilayers, multiplication of eqs 3a and 3b (or eqs 4a and 4b) was applied to explain the experimental results. Therefore, the spin labels were assumed to participate simultaneously in fast stochastic librations and in slow inertial rotations. The results of the present work shown in Figures 3 and 4 also may be interpreted in that way. Equations 3a and 4a determine the initial intercepting ($T = 0$), whereas eqs 3b and 4b describe the linear T-dependence of the $W(T)$ rate.

Note that conventional rotational Brownian diffusion via infinitesimal angular steps is characterized by a quadratic dependence on the time delay, τ,[20] which is certainly not the case for the results obtained here. (See Figure 3b.) As in our experiment, only small-angle reorientations manifest themselves, by angles less than 2°; this may imply that "infinitesimal" steps are in fact larger than 2°.

Because the data obtained at low peptide concentration (Figures 4a and 5a) do not show a noticeable T-dependence, we conclude that in that case the peptide experiences only fast librations near equilibrium positions that are described by eq

1. An increase in peptide concentration results in a remarkable *T*-dependence (Figures 4b and 5b), which becomes stronger with temperature increase. It may be interpreted as the onset of slow rotations described by eq 2.

The estimated characteristic rotational frequencies Ω_{slow} given in Figure 6 for both label positions are close. It may imply that peptide rotates like a solid cylinder. (For that case, instead of eqs 4 for isotropic motion, eqs 3 should be applied for uniaxial motion around a particular molecular axis.)

The onset of slow rotations at high peptide concentration may be associated with a change of the peptide orientation from the in-plane to the transmembrane one,[14,16] with the N-terminus going deeper into the membrane. In the transmembrane orientation, the peptide molecules are most probably aligned along the surrounding lipids, providing a freedom for motion around the peptide helix.

The CW EPR spectra shown in Figure 1 indicate the change of orientation because the splitting between two outer extremes shown for FTOAC1 becomes noticeably smaller at high peptide concentration, whereas for FTOAC8, it does not change. This diminishing of the splitting (observed also at low temperatures) may be attributed to decrease in the polarity in the surrounding of the spin label, which one must expect when the label is going deeper into the membrane.[30]

More direct information on the peptide orientation is provided by the ESEEM experiment presented in Figure 2. As was mentioned above, it may be readily interpreted as a consequence of a change of the in-plane to the transmembrane peptide helix orientation, with a deeper insertion of the N-terminus (including the hydrophobic Fmoc group) into the membrane interior. One more important feature seen on the spectra in Figure 2 is that the drop of the intensity with increasing peptide concentration for FTOAC1 is accompanied by a remarkable decrease in the quadrupole doublet amplitude. This doublet is known to be observed only for distant D_2O molecules located farther than 0.5 nm away from the spin label.[24] Therefore, the presence of this doublet indicates the presence of the nearby free water molecules. The diminishing of the doublet amplitude indicates the absence of free water near the label, which additionally supports the conclusion that upon the increase in the peptide concentration the N-terminus of the peptide is buried in the membrane interior.

The fact that the deuterium peak does not completely disappear with the increase in concentration means that a few water molecules still exist nearby the spin label (at a distance smaller than 0.5 nm; see the model calculations presented in ref 24). Probably, water molecules are captured by the peptides, thereby forming a polar channel for transportation of polar molecules.

To prove that during sample preparation the contact of peptide with deuterium water did not result in hydrogen substitution by deuterium, a control ESEEM experiment was done with spin-labeled analogues prepared in the way described in the Materials and Methods Section. In this experiment, for both cases of FTOAC1 and FTOAC8 samples, deuterium ESEEM was not detected. It proves that detection of the "close" water in the described ESEEM experiment was not an artifact.

Previous PELDOR measurements on FTOAC1 in DPPC bilayer[14] have shown that at high concentration peptide molecules are aggregated, forming clusters of about two peptides each. As it has been already mentioned, CW EPR spectrum of FTOAC1 sample shown in Figure 1c gives strong evidence that two N-terminal spin labels are mutually in close contact. In combination with the ESEEM data indicating the transmembrane orientation of these peptides, we may conclude that the two peptides of the dimer are located in opposite leaflets of the bilayer.

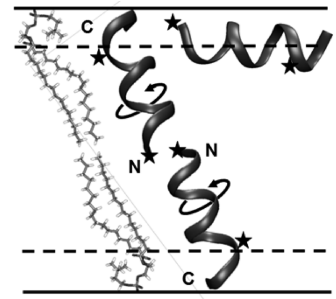

Figure 7. Topologies of the FTOAC peptides at the surface of the membrane at low peptide concentration and the head-to-head associated transmembrane dimer at high concentration. The circular arrows show molecular rotation. The stars indicate the positions of spin labels at the side chains of the TOAC residues, which were taken from an X-ray crystal structure.[37] This simple model suggests a transport mechanism through possible water channels located at the interface between the peptide and the membrane interior to overcome the membrane barrier.

In Figure 7, schematic model is depicted to visualize our experimental results. From fluorescence and molecular dynamics experiments, it is known that after the addition of trichogin GA IV to the outside of the membrane, the molecules self-associate to both the inner and outer leaflets of the membrane, even at low concentration.[16,31] Therefore, it is likely to suggest that at high peptide concentration the molecules self-associate to form head-to-head transmembrane dimers,[13] the length (~4 nm) of which would match the thickness of the double layer. It is worth noting that this kind of dimerization is similar to the manner of association of the channel-forming peptide gramicidin A.[32−36] In the case of trichogin GA IV, however, the peptide molecules do not have enough space inside the α-helices to allow ion transport compared with the much wider pores of the β-helices of gramicidin A. Moreover, trichogin GA IV is known to induce membrane leakage for larger polar molecules, like carboxyfluorescein.

A possible explanation of the membrane-modifying properties of trichogin GA IV could be that the rotational mobility of the peptide helices promotes transport of polar molecules in the membrane acting like a hole-drilling device. Our ESEEM experiment with FTOAC1 at $P_{SL}/P/L$ ratio of 1:9:200 (Figure 2) supports this model because here the water-spin label accessibility is not zero (albeit limited).

Of course, at physiological temperatures, other types of rotational motion appear that may superimpose the motion found here at cryogenic temperatures. The key point, however, is that the latter is not a conventional Brownian rotation but an inertial rotation. Such a rotation implies that peptides rotate like a motor, which may provide a principally new mechanism of driving molecular transport across the membrane.

Conclusions

In the stimulated ESE experiments of the present work, we find that at low peptide concentration the spin labels attached to the peptides show only a fast (nanosecond) librational type of motion for the nonaggregated molecules that are located at the membrane surface. This motion was observed in the experimentally accessible temperature range below ~150 K. At high peptide concentration, also a slow (millisecond) rotational motion appears. The onset of slow motions might be related to

the change of peptide orientation from the in-plane to the transmembrane disposition, accompanying the change from the monomeric to the aggregated state. In the latter case, the helical peptide molecules are expected to align along the surrounding lipids, thus inducing freedom for motion around the direction of the peptide helix.

Because the TOAC nitroxide spin labels are rigidly incorporated into the peptide structure, the observed mobility may be assigned to the rotation of the peptide backbone. This rotation, in turn, might induce transport of small polar molecules.

Of course, the proposed mechanism needs further validation. Here we observed only small-angle rotations and, at the moment, we cannot conclude on the full reorientation of molecules, which is certainly needed to ascertain this mechanism to be operative. However, the small-angle rotations may serve as the elementary steps for these reorientations, and the obtained results may give a clue to further investigations.

Acknowledgment. We thank A. D. Milov and Yu. D. Tsvetkov for useful discussions. This work was financially supported by Presidium of RAS, project 55, by Ministry of Education and Science of RF, project 2.1.1/1522, by Siberian Branch of RAS, project 75, and the Dutch-Russian Research Cooperation Program (Netherlands Organization of Scientific Research in collaboration with the Russian Foundation of Basic Research), NWO 047.017.034.

References and Notes

(1) Auvin-Guette, C.; Rebuffat, S.; Prigent, Y.; Bodo, B. *J. Am. Chem. Soc.* **1992**, *114*, 2170–2174.

(2) Toniolo, C.; Crisma, M.; Formaggio, F.; Peggion, C.; Epand, R. F.; Epand, R. M. *Cell. Mol. Life Sci.* **2001**, *58*, 1179–1188.

(3) Peggion, C.; Formaggio, F.; Crisma, M.; Epand, R. F.; Epand, R. M.; Toniolo, C. *J. Pept. Sci.* **2003**, *9*, 679–689.

(4) Marshall, G. R. *Studies on the Biologically Active Conformation of Angiotensin*; Intra-Science Chemistry Report; Gordon & Breach: New York, 1971; Vol. 5, pp 305−316.

(5) Karle, I. L.; Balaram, P. *Biochemistry.* **1990**, *29*, 6747–6756.

(6) Toniolo, C.; Crisma, M.; Formaggio, F.; Peggion, C. *Biopolymers* **2001**, *60*, 396–419.

(7) Rebuffat, S.; Goulard, C.; Bodo, B.; Roquebert, M.-F. *Recent Res. Dev. Org. Biorg. Chem.* **1999**, *3*, 65–91.

(8) Kropacheva, T. N.; Raap, J. *Biochim. Biophys. Acta* **2002**, *1567*, 193–203.

(9) Stella, L.; Mazzuca, C.; Venanzi, M.; Palleschi, A.; Didonè, M.; Formaggio, F.; Toniolo, C.; Pispisa, B. *Biophys. J.* **2004**, *86*, 936–945.

(10) Benedetti, E.; Bavoso, A.; Di Blasio, B.; Pavone, V.; Pedone, C.; Toniolo, C.; Bonora, G. M. *Proc. Natl. Acad. Sci. U.S.A.* **1982**, *79*, 7951–7954.

(11) Nagaraj, R.; Balaram, P. *Acc. Chem. Res.* **1981**, *14*, 356–362.

(12) Sansom, M. S. P. *Prog. Biophys. Mol. Biol.* **1991**, *55*, 139–235.

(13) Monaco, V.; Formaggio, F.; Crisma, M.; Toniolo, C.; Hanson, P.; Millhauser, G. L. *Biopolymers.* **1999**, *50*, 239–253.

(14) Salnikov, E. S.; Erilov, D. A.; Milov, A. D.; Tsvetkov, Yu. D.; Peggion, C.; Formaggio, F.; Toniolo, C.; Raap, J.; Dzuba, S. A. *Biophys. J.* **2006**, *91*, 1532–1540.

(15) Epand, R. F.; Epand, R. M.; Monaco, V.; Stoia, S.; Formaggio, F.; Crisma, M.; Toniolo, C. *Eur. J. Biochem.* **1999**, *266*, 1021–1028.

(16) Mazzuca, C.; Stella, L.; Venanzi, M.; Formaggio, F.; Toniolo, C.; Pispisa, B. *Biophys. J.* **2005**, *88*, 3411–3421.

(17) Heuber, C.; Formaggio, F.; Baldini, C.; Toniolo, C.; Müller, K. *Chem. Biodiversity* **2007**, *4*, 1200–1217.

(18) Toniolo, C.; Crisma, M.; Formaggio, F. *Biopolymers* **1998**, *47*, 153–158.

(19) Bartucci, R.; Guzzi, R.; De Zotti, M.; Toniolo, C.; Sportelli, L.; Marsh, D. *Biophys. J.* **2008**, *94*, 2698–2705.

(20) Isaev, N. P.; Dzuba, S. A. *J. Phys. Chem. B.* **2008**, *112*, 13285–13291.

(21) Isaev, N. P.; Syryamina, V. N.; Dzuba, S. A. *J. Phys. Chem. B.* **2010**, *114*, 9510–9515.

(22) Chernova, D. A.; Vorobiev, A. Kh. *J. Polym. Sci., Part B: Polym. Phys.* **2009**, *47*, 107–120.

(23) Toniolo, C.; Crisma, M.; Formaggio, F.; Peggion, C.; Monaco, V.; Goulard, C.; Rebuffat, S.; Bodo, B. *J. Am. Chem. Soc.* **1996**, *118*, 4952–4958.

(24) Milov, A. D.; Samoilova, R. I.; Shubin, A. A.; Grishin, Yu. A.; Dzuba, S. A. *Appl. Magn. Reson.* **2008**, *35*, 73–94.

(25) Gordon-Grossman, M.; Gofman, Y.; Zimmermann, H.; Frydman, V.; Shai, Y.; Ben-Tal, N.; Goldfarb, D. *J. Phys. Chem. B* **2009**, *113*, 12687–12695.

(26) Salnikov, E. S.; De Zotti, M.; Formaggio, F.; Li, X.; Toniolo, C.; O'Neil, J. D. J.; Raap, J.; Dzuba, S. A.; Bechinger, B. *J. Phys. Chem. B* **2009**, *113*, 3034–3042.

(27) Erilov, D. A.; Bartucci, R.; Guzzi, R.; Marsh, D.; Dzuba, S. A.; Sportelli, L. *J. Phys. Chem. B* **2004**, *108*, 4501–4507.

(28) Toropov, Yu. V.; Dzuba, S. A.; Tsvetkov, Yu. D.; Monaco, V.; Formaggio, F.; Crisma, M.; Toniolo, C.; Raap, J. *Appl. Magn. Reson.* **1998**, *15*, 237–246.

(29) Nesmelov, Y. E.; Karim, C. B.; Song, L.; Fajer, P. G.; Thomas, D. D. *Biophys. J.* **2007**, *93*, 2805–2812.

(30) Derek, M. *Proc. Nat. Acad. Sci. U.S.A.* **2001**, *98*, 7777–7782.

(31) Bocchinfuso, G.; Palleschi, A.; Orioni, B.; Grande, G.; Formaggio, F.; Toniolo, C.; Park, Y.; Hahm, K.-S.; Stella, L. *J. Pept. Sci.* **2009**, *15*, 550–558.

(32) Roux, B. *Acc. Chem. Res.* **2002**, *35*, 366–375.

(33) Dzikovski, B. G.; Borbat, P. P.; Freed, J. H. *Biophys. J.* **2004**, *87*, 3504–3517.

(34) Hu, J.; Chekmenev, E. Y.; Gan, Z.; Gorkov, P. L.; Saha, S.; Brey, W. W.; Cross, T. A. *J. Am. Chem. Soc.* **2005**, *127*, 11922–11923.

(35) Xie, X.; Al-Momani, L.; Reiss, P.; Griesinger, C.; Koert, U. *FEBS J.* **2005**, *272*, 975–986.

(36) Chattopadhyay, A.; Rawat, S. S.; Greathouse, D. V.; Kelkar, D. A.; Koeppe, R. E. *Biophys. J.* **2008**, *95*, 166–175.

(37) Toniolo, C.; Peggion, C.; Crisma, M.; Formaggio, F.; Shui, X.; Eglleston, D. L. *Nat. Struct. Biol.* **1994**, *1*, 908–914.

JP106769Q